Natural Hazards Research 3 (2023) 531–545

Contents lists available at ScienceDirect

Natural Hazards Research

journal homepage: www.keaipublishing.com/en/journals/natural-hazards-research

Applying rainfall threshold estimates and frequency ratio model for landslide hazard assessment in the coastal mountain setting of South Asia

Akhtar Alam [a,b,*], Bayes Ahmed [b], Peter Sammonds [b], A.S.M. Maksud Kamal [c]

[a] Department of Geography and Disaster Management, University of Kashmir, Srinagar, 190006, India
[b] Institute for Risk and Disaster Reduction, University College London, Gower Street, London, WC1E 6BT, United Kingdom
[c] Department of Disaster Science and Climate Resilience, University of Dhaka, Dhaka, 1000, Bangladesh

ARTICLE INFO

Keywords:
Frequency ratio
Landslide susceptibility
Risk
Rainfall threshold
GIS
LEWS
South Asia

ABSTRACT

Landslides pose a serious risk to life and property in the mountainous regions around the globe. Understanding the interplay of landslide conditioning and triggering factors is essential for lessening the impacts caused by the hazard. Cox's Bazar — a coastal mountainous district in Bangladesh is recurrently affected by rainfall-triggered landslides. Based on analysis of 14 experiential landslides and combination of gauged and satellite rainfall estimates for the period from 2003 to 2019, the present study determines three landslide-triggering rainfall thresholds for the Cox's Bazar District (CBD): 1. Intensity-Duration (ID) threshold derived in this study revealed that any rainfall event with an intensity of ≥4.04 mm/h if prolonging for ≥12h can cause slope failures; 2. Event-Duration (ED) threshold suggested that a normalized cumulative event rainfall (E_{MAP}) of 0.15 for one day is expected to trigger landslides; and 3. threshold calculated using randomly chosen antecedent rainfall expressed best distinction on 30-day rainfall and the equation of the threshold came out as R_{th} = 64–0.02 R_a30. The recurrence probability of the derived antecedent rainfall threshold and likely landslides was determined through the Poisson distribution. Moreover, we assess the landslide susceptibility of the district with a coupled use of Frequency Ratio (FR) statistical measure and Geographic Information System (GIS). Considering the combined role of selected conditioning factors, the landslide susceptibility status of the CBD was quantified and classified into probability intervals. The accuracy of the susceptibility maps was assessed through the Relative Landslide Density Index (R-Index) that used a field landslide inventory, comprising well distributed 891 events. Moreover, gridded population data was superimposed on the derived susceptibility maps to understand the risk levels of people. The derivation of landslide-triggering rainfall thresholds and spatial susceptibility assessment has been useful to propose a low-cost Landslide Early Warning System (LEWS) which can contribute in alleviating the adverse effects of landslide hazard in the CBD.

1. Introduction

Landslide is an inclusive term for a range of downslope movements of rock and soil material under the influence of gravity. Based on the type of movement and the material involved, landslides are classified into different types (e.g., Varnes, 1978). Variety of factors such as slope, lithology, soil, land cover, rainfall and human interventions contribute to the occurrence of landslides (Alexander, 1992; Baeza and Corominas, 2001). Landslides are most common natural hazard in mountainous environments, causing immense loss of human life and infrastructure each year. The hazard is also a common cause of disruption to land transportation and utility services. In the recent past, there has been a multifold increase in the impacts from the landslides owing to continuous increase in the population and development activities, particularly in the mountainous areas (Van Westen et al., 2012; Bogaard and Roberto, 2018; Shah et al., 2022). The hazard accounted for 4.89% of the total disasters that occurred worldwide during the years 1990–2005 (www.em-dat.net). Globally 2620 nonseismically triggered landslides caused a total of 32,322 fatalities between the period from 2004 to 2010 (Petley, 2012). From 1995 to 2014, landslides (3876 events) caused 163,658 deaths and 11,689 injuries globally with more than half of the events in areas receiving high rainfall (Haque et al., 2019). About 54% of the landslide events between 1990 and 2015 occurred in Asia (Guha-Sapir et al., 2018) and the continent bears most of the human losses particularly along the

* Corresponding author. Department of Geography and Disaster Management, University of Kashmir, Srinagar, 190006, India.
E-mail address: alamakhtar@uok.edu.in (A. Alam).

https://doi.org/10.1016/j.nhres.2023.08.002
Received 21 June 2023; Received in revised form 18 August 2023; Accepted 18 August 2023
Available online 21 August 2023
2666-5921/© 2023 National Institute of Natural Hazards, Ministry of Emergency Management of China. Publishing services provided by Elsevier B.V. on behalf of KeAi Communications Co. Ltd. This is an open access article under the CC BY-NC-ND license (http://creativecommons.org/licenses/by-nc-nd/4.0/).

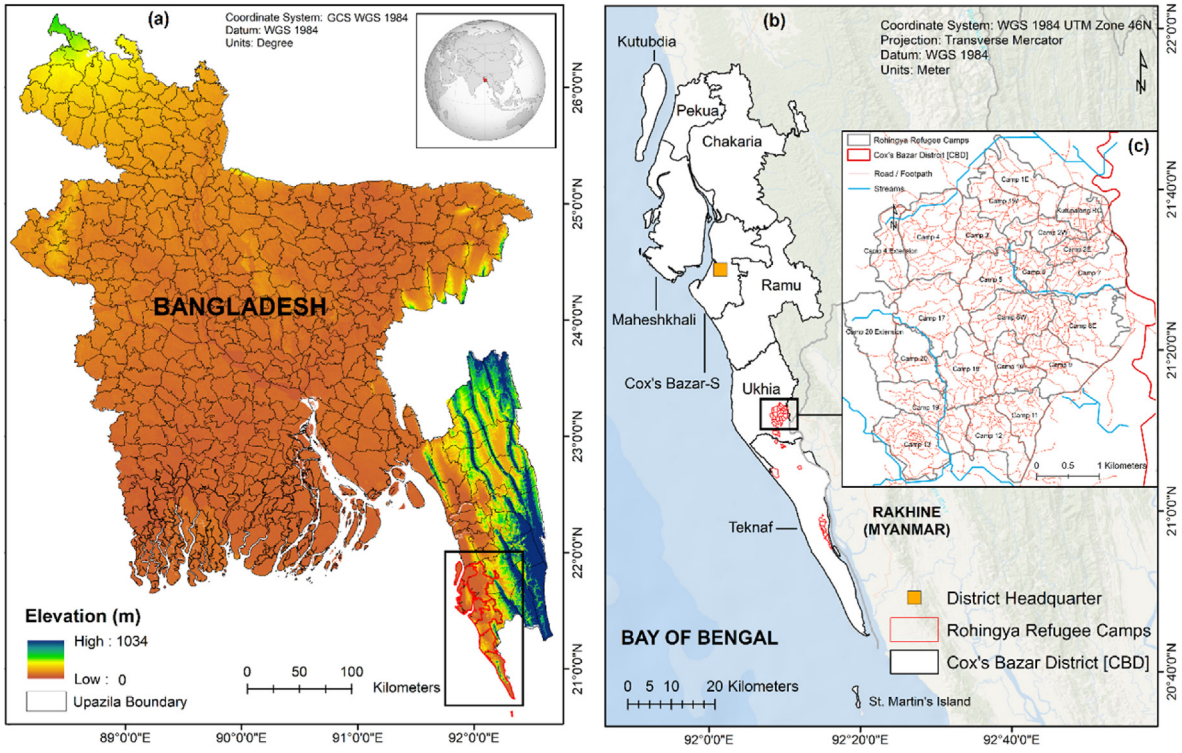

Fig. 1. Location of the study area. (a) Bangladesh, (b) Cox's Bazar District (CBD), (c) Rohingya Refugee Camps.

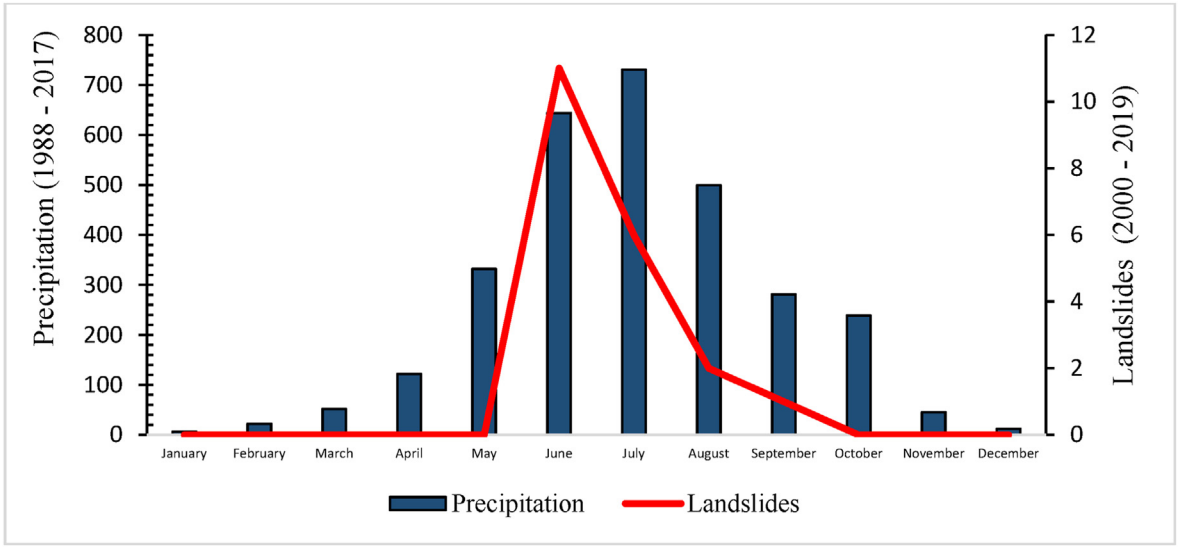

Fig. 2. Pattern of mean monthly precipitation and landslide occurrence in the CBD.

Himalayan mountain region (Petley, 2012). The economic loss and the causalities caused by the landslides are substantially more than what is normally recognized (Schuster and Highland, 2001; Ali et al., 2022).

Landslides are recurrent hazard in the hilly districts [Khagrachari, Rangamati, Chittagong, Cox's Bazar, and Bandarban] of Bangladesh (Ahmed 2015; Ahmed, 2017; Ahmed et al., 2020). Historical record of landslide events (2000–2018) reveals that on an average 19 landslides occur annually in the country with an increase of 4% each year (Sultana, 2020). A single rainfall event triggered 100 landslides on the 11th of June 2007 resulting in death of 127–135 people (Sarwar, 2008). Other deadly landslide events in the country are that of 15 June 2010, 27 June 2012, and 13 June 2017 with a death toll of 57, 96, and 164 respectively (Sultana, 2020). Besides being susceptible to landslide hazard, socioeconomic factors such as poverty, demographic composition and land utilization patterns (e.g., rampant hill cutting) and human settlement expansion have been important factors exacerbating landslide risk of the people (Ahmed and Dewan, 2017; Alam et al., 2019; Ahmed et al., 2020).

While rainfall remains the most common cause of landslides across the continents, the intensity of the rainfall events is likely to increase or double in the wake of changing climate which in turn enhances the probability of landslide occurrence and associated losses (Wu et al., 2015; Gariano and Guzzetti, 2016; Park et al., 2019; Dunbar, 2019; Ahsan et al., 2021, 2023). Correlating the precipitation and landslide trends in the future (2061–2100), a recent report (NASA Earth Observatory, 2020) projected an increase of 30–70% in the landslide events

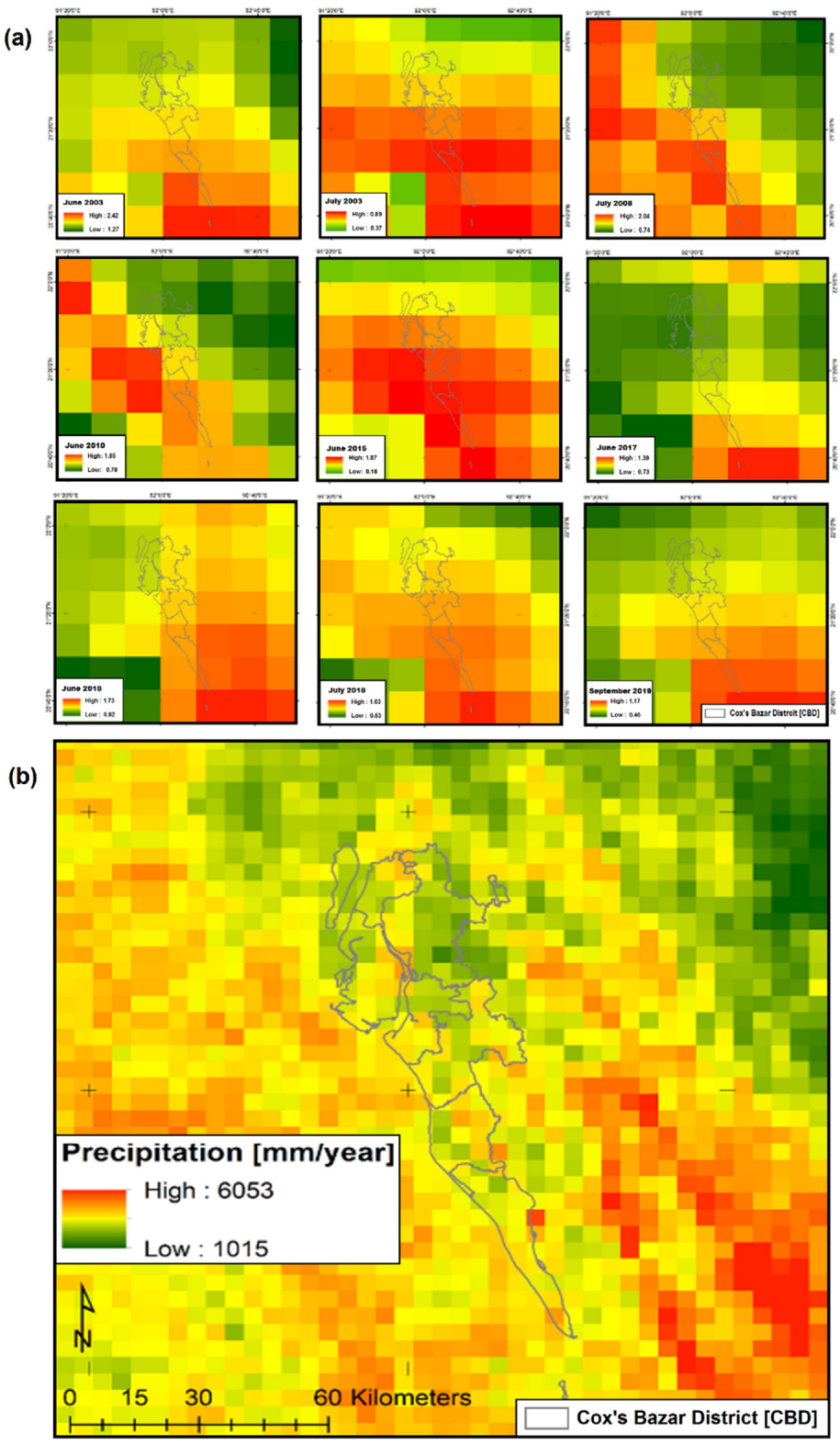

Fig. 3. TRMM precipitation estimates of the Cox's Bazar District (CBD) and neighbouring areas. (a) rainfall estimate [L3 1 month 0.25° × 0.25° V7] for the months that witnessed landslides and (b) mean annual precipitation.

over the Himalayan region. In view of the anticipated scenarios, deriving landslide-triggering rainfall thresholds, assessing landslide susceptibilities and developing reliable Landslide Early Warning Systems (LEWS) at various spatial scales is of immense importance for reducing the losses from the hazard.

Multivariate analysis is widely used for landslide susceptibility analysis in which a landslide is considered as function of the relationship between multiple environmental factors that vary in space and time (Baeza and Corominas, 2001). A range of statistical and machine learning models such as Logistic Regression (LR), Frequency Ratio (FR), Analytic Hierarchy Process (AHP), Fuzzy Logic, and Artificial Neural Networks (ANN) have long been used in combination with Geographic Information

Table 1
Rainfall sequence of the experienced landslides (2003–2019).

Date	*Event Duration [Days]*	*Cumulative Rainfall [mm]*	E_{MAP}
16 June 2003	12	474	0.18
29 July 2003	11	330	0.12
03 July 2008	7	688	0.26
06 July 2008	10	981	0.37
07 April 2010	–	No data	–
15 June 2010	6	523	0.19
26 June 2015	4	978	0.37
28 June 2015	5	674	0.25
27 July 2015	6	682	0.25
13 June 2017	1	300	0.11
25 July 2017	6	677	0.25
11 June 2018	4	459	0.17
12 June 2018	–	No data	–
25 July 2018	1	228	0.08
10 September 2019	1	422	0.16

System (GIS) for landslide susceptibility analysis (e.g., Ayalew and Yamagishi, 2005; Lee, 2005; Yesilnacar and Topal, 2005; Brenning, 2008; Yilmaz, 2009; Chauhan et al., 2010; Park et al., 2013; Wang et al., 2013; Lin et al., 2017; Lombardo and Mai, 2018; Rahman et al., 2020). The relative weight estimation of each contributing factor through these statistical models and overlay capability of GIS allows integration of factor layers in different ways to develop susceptibility maps (Baeza and Corominas, 2001; Huabin et al., 2005).

The present work aims to derive multiple landslide-triggering rainfall thresholds and assess the landslide susceptibility based on range of conditioning factors in the Cox's Bazar District (CBD). The analysis has been carried out through a series of sequential steps that include: evaluation of relationship between rainfall characteristics and landslide occurrence, estimation of three different rainfall thresholds that can trigger landslides, selection of factors that contribute to landslide susceptibility, development of respective GIS layers, determining the relative importance of each layer through the statistical measure (FR), development and validation of the susceptibility maps, and integration of population data with susceptibility maps for simulating the risk scenario. Finally, based on the obtained results, a LEWS is proposed for the study area. On the whole the output of this investigation can be useful in understanding the various dimensions of landslide hazard and minimizing the associated losses in the CBD.

2. Study area

Cox's Bazar district (CBD) forms the southern part of Chittagong Division of Bangladesh consisting of eight administrative units (Fig. 1). The district is spread over 2200 square kilometers with an elevation ranging from 0 to 263 m above mean sea level. The average annual rainfall in the CBD varies from 2400 to 2800 mm in the north to 3001–3500 mm in the south. A gradual increase is noticeable in the rainfall totals over the last 50 years in Bangladesh. The CBD is experiencing high landslide activity, causing human casualties and economic losses. Although factors related to land use pattern and poor management practices play a substantial role in enhancing landslide susceptibility, the landslide are mostly associated with the extreme rainfall events in the CBD particularly during the monsoon season (Fig. 2). Nearly 80% of the landslides occur during the summer months with most (30%) in the month of June (Khan et al., 2012). The lithology of the area consists of beach and dune sand (Coastal sediments), valley alluvium and colluvium, Dihing and Dupi Tila Formation, Dihing Formation (Pleistocene and Pliocene), Tipam Sandstone (Neogene), Boka Bil Formation (Neogene) and Bhuban Formation (Miocene) (GSB, 1990). In addition to native population, the CBD is home to about 0.8 million Rohingya refugees (Fig. 1). The influx of Rohingya refugees and building of camps resulted in removal of extensive vegetation cover and increased the probability of landslide occurrence especially during rainfall events (Dunbar, 2019).

3. Materials and methods

3.1. Derivation of rainfall thresholds

Empirical rainfall thresholds are broadly categorized into three types: (i) event based that use records of a particular rain event (ii) antecedent rainfall based and (iii) alternate thresholds that include hydrological thresholds (Guzzetti et al., 2007; Baum et al., 2018). In this analysis we derived three landslide inducing rainfall thresholds: 1. Intensity-Duration (I-D) and 2. Event-Duration (E-D) and 3. Antecedent Precipitation thresholds using satellite rainfall [JAXA Global Rainfall Watch (GSMaP), Tropical Rainfall Measuring Mission (TRMM)] and gauge rainfall data from the Bangladesh Meteorological Department (BMD). Record of 14 landslides with known date of occurrence experienced in the study area for the period between 2003 and 2019 and corresponding rainfall estimates were used for the analysis (Fig. 3, Table 1).

3.1.1. Intensity-duration (I-D)

I-D thresholds are preferred and most widely proposed type of the thresholds (Robbins, 2016). They are generally expressed by a power law (Eq. (1)):

$$I = c + \alpha \times D^{\beta} \tag{1}$$

where I is rainfall intensity, D is rainfall duration, and c, α and β are fitting parameters (Martinović et al., 2018). Rainfall intensity implies the amount of precipitation accumulated in a period, or the rate of precipitation in a period, most commonly measured in millimeters (or inches) per hour (Guzzetti et al., 2007).

Table 2
Accumulated rainfall prior to landslide events; maximum intensity [mm/h] represents highest value recorded within 30 days before a landslide.

Date	*ID*	*12h*	*24h*	*72h*	*1w*	*2w*	*1m*	*Maximum Intensity*
16 June 2003	L1	8.2	10.7	31.3	468.7	898.4	991.7	26.47
29 July 2003	L2	14.3	14.3	21.5	46.3	75.7	152.8	5.27
03 July 2008	L3	30.7	53.2	178.3	345.5	416	626	6.48
06 July 2008	L4	45.4	81.2	157.6	370.5	512	749.9	7.83
15 June 2010	L5	146.2	218.1	406.8	431.9	486.6	929.6	18.74
26 June 2015	L6	95.4	135.1	561.3	731.8	797.5	1014	37.32
28 June 2015	L7	0.6	15.9	241.9	832.7	881.3	1122.6	37.32
27 July 2015	L8	18.3	78.2	337.7	414.5	542.2	752.1	15.23
13 June 2017	L9	38.2	88.4	215.2	317.2	354.9	522.1	8.03
25 July 2017	L10	46.9	134.2	280	439.7	484	742.8	10.93
11 June 2018	L11	65.8	121.7	233	249.5	324	451.9	15.91
12 June 2018	L12	83.2	105.1	317.5	348.9	420.7	512.4	15.91
25 July 2018	L13	50	81.9	141.2	151	184	342.1	6.50
10 September 2019	L14	37	46.7	118.7	140.8	236.5	440.7	5.83

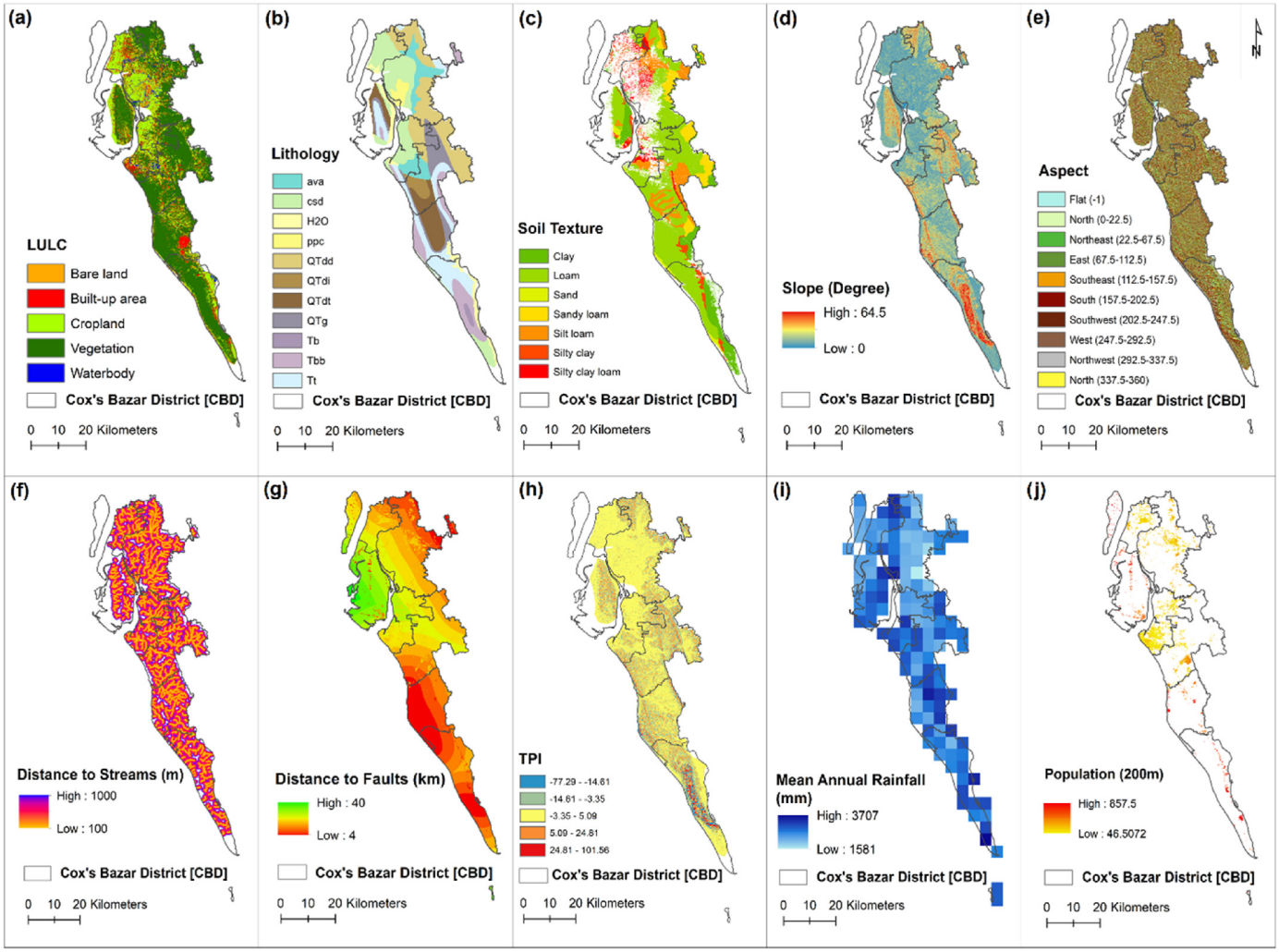

Fig. 4. Factors selected for the landslide susceptibility and risk assessment. Details of lithology, ava: Valley alluvium and colluvium, csd: Beach and dune sand, Ppc: Marsh clay and pea, QTdd: Dihing and Dupi Tila Formation Undivided, QTdi: Dihing Formation (Pleistocene and Pliocene) QTdt: Dupi Tila Formation (Pleistocene and Pliocene), QTg: Girujan Clay (Pleistocene and Neogene), Tb: Bhuban Formation (Miocene), Tbb: Boka Bil Formation (Neogene), Tt: Tipam Sandstone (Neogene).

3.1.2. *Event-Duration (E-D)*

The *E-D* threshold adopted here considers normalized cumulative event rainfall (E_{MAP}), a unit less parameter expressed as Eq. (2).

$$E_{MAP} = E/MAP \tag{2}$$

Where E is the cumulative event rainfall and MAP is the mean annual precipitation (Sengupta et al., 2010).

3.1.3. *Antecedent rainfall*

Antecedent precipitation effects the ground water, soil moisture conditions and landslide occurrence. The rainfall estimates preceding a landslide event are made using Eq. (3).

$$AP_x = R_1 + R_2 + \ldots + R_n \tag{3}$$

where AP_x is cumulative antecedent rainfall for day *x;* R_1 is the rainfall amount for the day before *x;* R_n is the daily rainfall amount for the *n*th day before day *x*. Table 2 shows the details of antecedent rainfall of the selected landslide events.

3.2. *Susceptibility mapping*

This study used range of landslide influencing factors that include land use and land cover, lithology, soil, slope, aspect, distance to streams, distance to faults, topographic position index (TPI), and rainfall for landslide susceptibility analysis of the CBD (Fig. 4). The selected data layers have been identified as the fundamental requirements for the landslide susceptibility in different studies (e.g., Lee, 2005; Yilmaz, 2009; Park et al., 2013; Wang et al., 2013; Lin et al., 2017; UNISDR, 2017; Huang et al., 2018; Lombardo and Mai, 2018). Relative weight of the selected factors was determined through Frequency Ratio (FR) model and subsequently used in GIS for overlay analysis and developing the susceptibility map. Moreover, the present analysis makes use of comprehensive field based landslide inventory. Generated using handheld Global Positioning System (GPS), the inventory has been of great value to assess the accuracy of the generated landslide susceptibility map. Moreover, data about the population density has also been used to project the likely impacts on the inhabited parts of the CBD. The characteristics and sources of the datasets used in the present study are given in Table 3.

3.2.1. *Frequency ratio model*

Frequency ratio (FR) statistical analysis is based on the observed relationships between distribution of landslides and the factors influencing the landslide occurrence (Lee and Pradhan, 2007). The FR is a ratio of the area where landslides have occurred to the total area; a value greater than 1 implies higher correlation, and value lower than 1 is suggestive of lower correlation. The frequency (FR) ratio of each landslide factor class

Table 3
Characteristics of the selected data layers. LULC: Land use and Land cover, OLI: Operational Land Imager (2020), SRTM: Shuttle Radar Topography Mission, DEM: Digital Elevation Model, TRMM: Tropical Rainfall Measuring Mission.

Factor	*Scale and Pixel size*	*Data product used*	*Source*
LULC	30m	Landsat-8 OLI image	https://glovis.usgs.gov/
Lithology	1:50,000/ 30m	Surface Geology Map	https://pubs.usgs.gov/
Soil	1:50,000/ 30m	Soil Map	http://www.srdi.gov.bd/
Slope (degrees)	30m	SRTM DEM	https://earthexplorer.usgs.gov/
Aspect (Orientation)	30m	SRTM DEM	https://earthexplorer.usgs.gov/
Distance to streams (m)	30m	SRTM DEM	https://earthexplorer.usgs.gov/
Distance to faults (km)	30m	Surface Geology Map	https://pubs.usgs.gov/
TPI (-77–102)	30m	SRTM DEM	https://earthexplorer.usgs.gov/
Rainfall (mm)	4000m	TRMM	https://mirador.gsfc.nasa.gov/
Population (density)	90m	Number of people per grid cell or 100 m)	https://www.worldpop.org/geodata/

was calculated using Eq. (4).

$$FR = \frac{Npix\ (S_i) / \sum Npix\ (S_i)}{Npix\ (N_i) / \sum Npix\ (N_i)} \tag{4}$$

where *Npix* (S_i) is the number of pixels with landslides in factor class *i*, Σ *Npix* (S_i) is the total number of pixels with landslides, *Npix* (N_i) is the total number of pixels in factor class *i*, Σ *Npix* (*Ni*) is the total number of pixels in entire area of interest. The landslide susceptibility of an area is finally derived from the summation of the frequency ratios of all the selected landslide causing factors (e.g., Huang et al., 2018; Javier and Kumar, 2019); see Eq. (5).

$$LSI = FR_1 + FR_2 + FR_3 + \ldots + FR_n \tag{5}$$

3.3. Probability of landslide occurrence

In order to project the future occurrence of the landslides Poisson probability model expressed as Eq. (6) was used with two assumptions: (i) landslide occurrence is a function of rainfall exceeding the threshold, and (ii) there is no possibility or limited probability of landslide occurrence when rainfall amount is less than the threshold (e.g., Crovelli, 2000; Das et al., 2011; Bui et al., 2013; Dikshit et al., 2020).

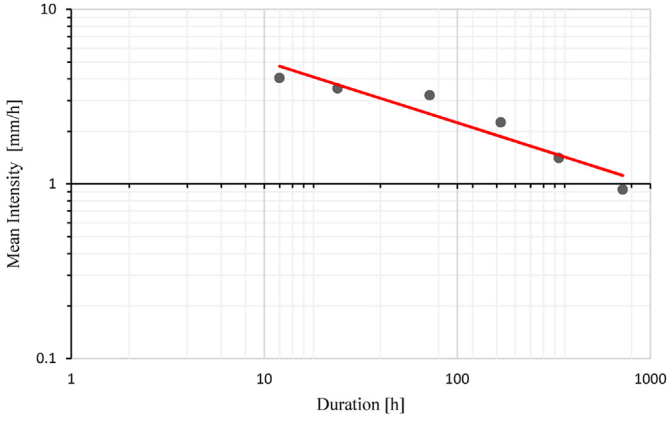

Fig. 5. Intensity-Duration threshold for the Cox's Bazar District (CBD).

$$P(N(t) = n) = e^{-\lambda t}\ \frac{(-\lambda t)^n}{n!};\quad n = 1, 2, 3, \ldots \tag{6}$$

where, N is the total number of landslides that occur during a time *t*; and λ is the rate of occurrence of landslides.

Probability of one or more landslides occurring during time *t*, which is the exceedance probability, can be estimated through Eq. (7).

$$P(N(t) \geq 1) = 1 - Exp\ (-t / \mu) \tag{7}$$

where μ is the future mean recurrence interval ($\mu = t^{-1}$); t is the future time period for which the exceedance probability is calculated. The future mean recurrence interval is estimated using the historical mean recurrence interval with the assumption that the future occurrence of landslides will remain the same as it was in the past (Crovelli, 2000; Bui et al., 2013). The frequency of the derived antecedent rainfall threshold observed in the past was used to simulate the return period and probability of the future landslides in the CBD.

4. Results

4.1. Intensity-duration (I-D)

The intensity-duration pattern of all the selected rainfall events was plotted at range of time intervals prior to a landslide event. The process involved two normalizations; in the first one, intensities were obtained by way of dividing accumulated rainfall by the time period and second one involved averaging of normalized values of each landslide event. Thus, the intensity values used do not represent the actual intensities, rather the values are average of the respective intervals. This way of using normalized intensities often underestimates the peak intensity values; however, it is may be beneficial for filtering out the anomalous minimum thresholds where actual triggering factor may be associated with a rare in-situ conditioning factor; a condition not representative of a wider area and a likely cause for generating the false alarm. Here we observe that any rainfall episode that continues for 12h with an intensity of ≥4.04 mm/h is likely to activate landslides in the Cox's Bazar District (Fig. 5). As the rainfall duration increases, the landslides are expected to be triggered by the low rainfall intensities. The threshold derived in this analysis was observed to be very close to the I-D threshold (4 mm/h for 12 h) calculated for the Garhwal Himalaya (Mathew et al., 2014).

4.2. Event-Duration (E-D)

The E-D sequence includes events of 1-day to 12-day duration with rainfall ranging from 228 mm to 981 mm (Table 1) having insignificant relationship between landslide occurrence and event duration. Considering Eq. (2) where value of E is normalized by dividing it by the MAP (2630) of the area, the E_{MAP} threshold was found to be 0.12. Thus, it is inferred that any rainfall event with the E_{MAP} value of 0.12 having duration of 1 day is likely to trigger landslides in the CBD. Using TRMM rainfall estimates, E_{MAP} threshold has also been developed with better spatial resolution for different parts of the district (Fig. 6). The scenario was derived by classifying the CBD into five zones with variable average annual rainfall patterns. Considering the average annual rainfall of each zone i.e., 1924 mm, 2401 mm, 2703 mm, 3013 mm and 3419 mm and the lower limit of the differentiating rainfall (330 mm) required to initiate the landslide in each rainfall zone of the district, the E_{MAP} for the zones has been found to be 0.20, 0.16, 0.14, 0.13 and 0.11 respectively (Fig. 6).

4.3. Antecedent rainfall

In general, antecedent rainfall thresholds are determined by correlating the daily and antecedent rainfall of the past landslide events; and the lower envelope of the interval revealing best separation between the

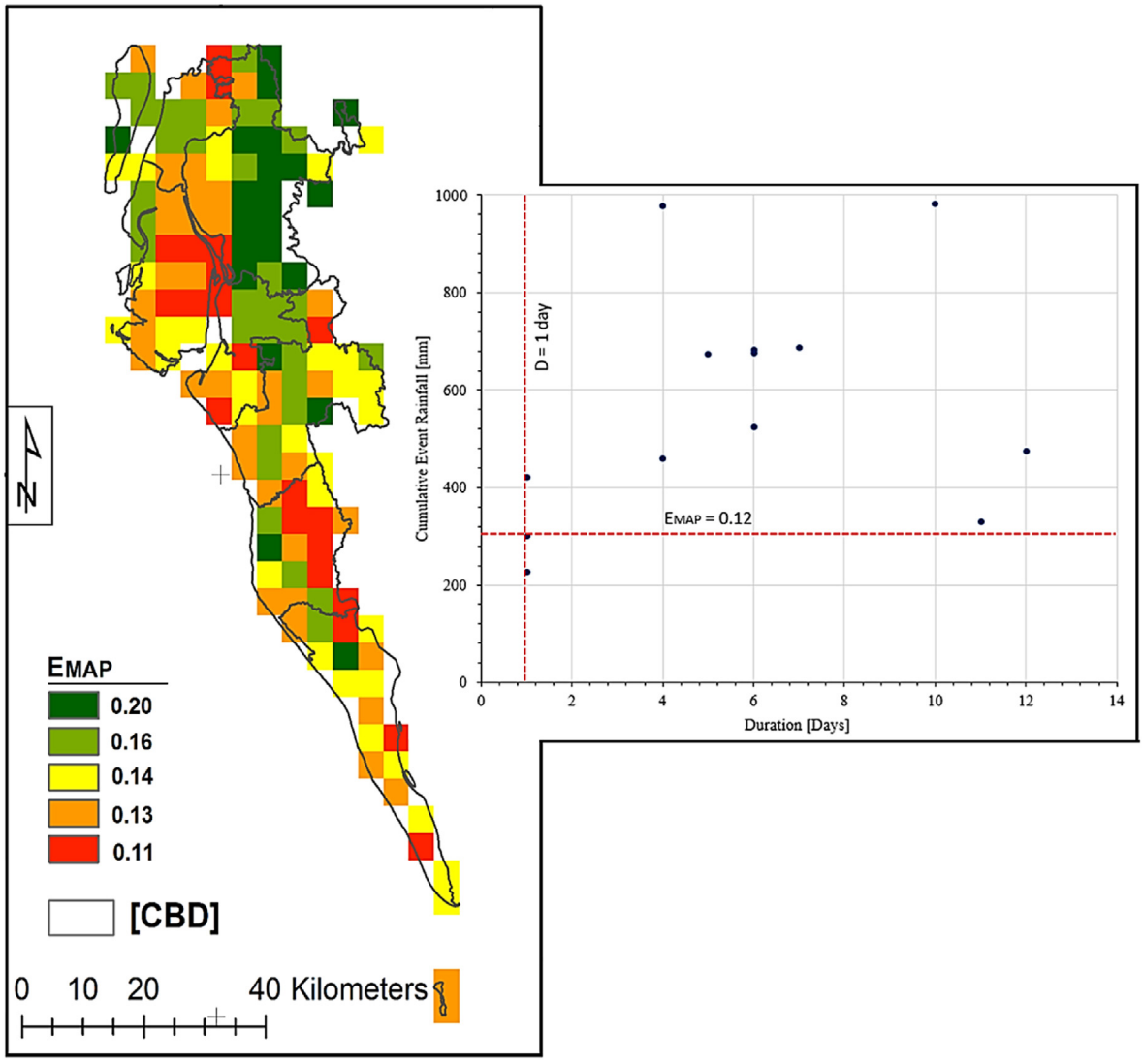

Fig. 6. Event-Duration rainfall threshold for the Cox's Bazar district. The spatial pattern of the E_{MAP} (left) has been developed on the basis of TRMM precipitation estimates; the scatter plot (right) shows the threshold value for the whole district.

two is chosen as a threshold (Chleborad 2003; Bui et al., 2013; Dikshit et al., 2020). However, main complexity in using antecedent precipitation for predicting landslides is to determine the accumulation period or the number of days (Guzzetti et al., 2007). Usually, a time period ranging from few days to few weeks is considered. In this study, the rainfall threshold was developed on the basis of daily rainfall and cumulative antecedent rainfall of the landslide events experienced in the CBD from 2003 to 2019. This way of threshold determination evaluates two components i.e., pre-existing water within the slope and triggering rain received on the day of landslide occurrence (Glade et al., 2000). Antecedent rainfall at four time intervals [3, 7, 14, and 30 days] corresponding to each landslide recorded before the event was used; see Table 2. Comparison of the maximum yearly rainfall in one day without landslides and antecedent rainfall estimates on a single axis revealed clear distinction at 30-day antecedent rainfall conditions (Fig. 7). Therefore, for deriving the threshold (R_{th}), daily rainfall with landslides and corresponding 30-day antecedent rainfall was correlated on a scatter plot; the mathematical equation of the lower limit of the curve came out to be $R_{th} = 64–0.02\ R_a30$; where, R_{th} is the rainfall threshold and R_a30 is the 30-day antecedent rainfall (Fig. 8). Based on the derived antecedent rainfall threshold, the probability and the return period of future landslides is derived as shown in Fig. 9.

4.4. Landslide susceptibility

The spatial patterns of landslide susceptibility have been illustrated through the generation of susceptibility map. The map is primarily composed of 30 × 30 m pixel matrix with a qualitative scale of landslide occurrence probability. The results of the statistical analysis i.e., the frequency ratios and the weightage of each factor is presented in Table 4. The levels of the susceptibility range from low to very high (Fig. 10). The percentage of area under different susceptibility classes has been 13.67% (low) 52.94% (moderate), 30.4% (high) and 2.99% (very high) respectively. The landslide susceptibility scenario created is fundamentally based on two assumptions: (i) the landslide occurrence is a function of the selected conditioning factors and (ii) the occurrence of future landslides would be governed by the same factors. The analysis provides an understanding of spatial distribution of future landslide occurrence; the identified 'very high' and 'high' landslide susceptibility areas are likely to experience enhanced landslide activity than the areas exhibiting 'moderate' and 'low' susceptibility. There is no consistent spatial pattern in the landslide susceptibility levels of the CBD, the scenario on the whole is sporadic in nature. However, the mountainous areas from the south of CBD (Teknaf) and steep slopes along the coast especially that of Ramu and Cox's Bazar-S sub-districts revealed 'very high' probability of

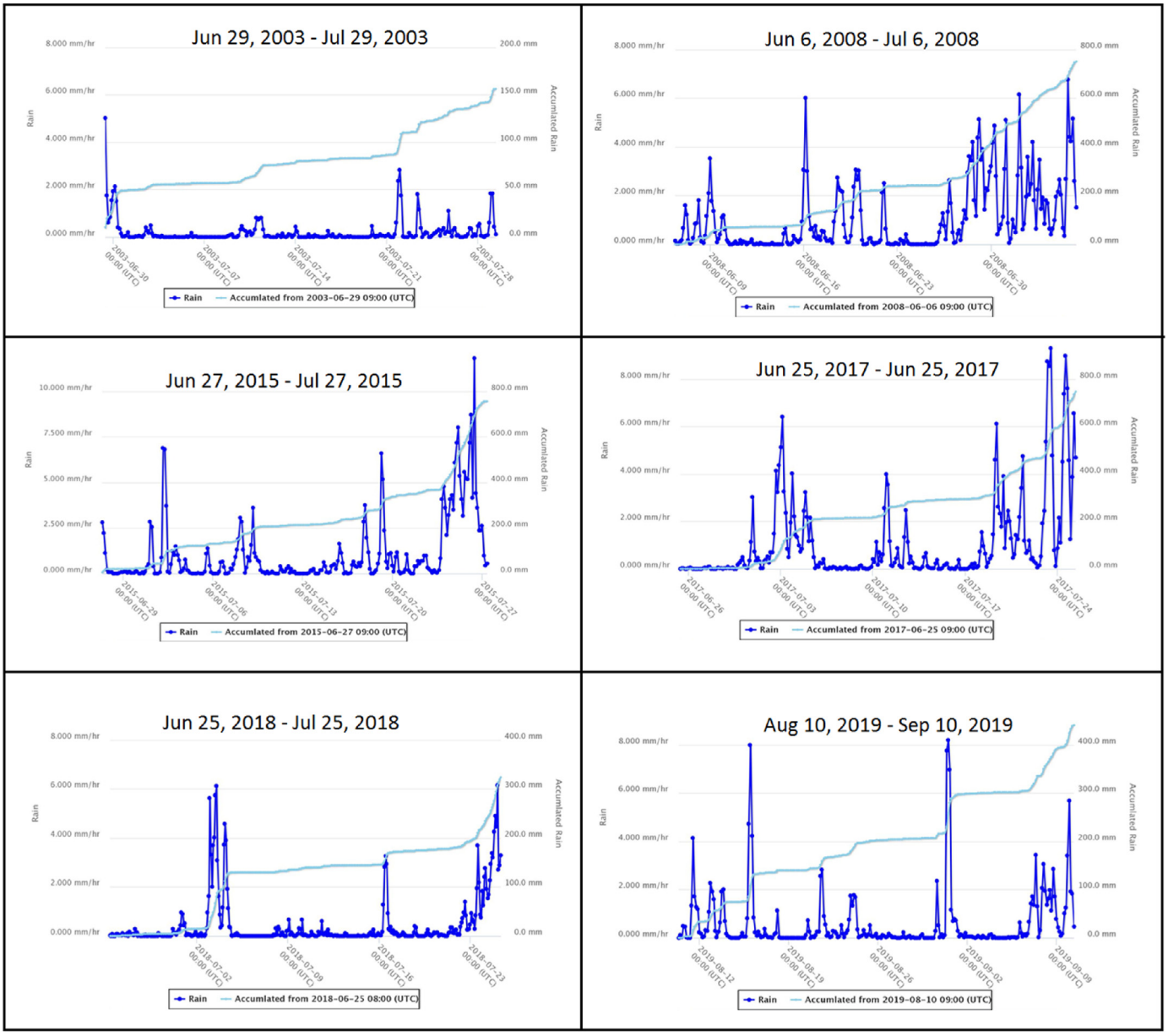

Fig. 7. 30-day accumulated rainfall and rainfall on the selected landslide days in the Cox's Bazar District (CBD) between 2003 and 2019; (Source: JAXA GSMaP).

landslides. The scattered flat areas of Chakaria, Maheshkhali, Cox's Bazar-S, Ramu and Ukhia, exhibited 'low' susceptibility levels (Fig. 10).

4.5. Validation of the susceptibility map

The accuracy of the landslide susceptibility simulations using various statistical models such as Frequency Ratio (FR), Logistic Regression (LR), Artificial Neural Networks (ANN), and Analytic Hierarchy Process (AHP) has not been observed to be consistent. For example, the accuracy of FR has been reported to be relative better than LR (e.g., Lee and Sambath 2006; Solaimani et al., 2013) and ANN (e.g., Poudyal et al., 2010) in some studies, whereas the same model (FR) has been found demonstrating almost similar accuracy compared to the LR, ANN and AHP (e.g., Park et al., 2013). The variability in the accuracy is usually associated with the selection of the landslide influencing factors, quality of the data used, and user bias. Here in the present analysis we assess the quality of the susceptibility map using relative landslide density index (R) Eq. (8) (e.g., Baeza and Corominas, 2001; Shahabi and Hashim, 2015).

$$R = \left(\frac{ni}{Ni}\right) \Big/ \sum \left(\frac{ni}{Ni}\right) \times 100 \quad (8)$$

where *ni* the number of landslides occurred in the susceptibility class *i* and *Ni* the number of pixels in the same susceptibility class *i*. The index is used to understand the correlation between the landslide susceptibility classes and landslide inventory. The results expressed a reasonable agreement with the observed landslides. (Fig. 11). The ratio of area under landslide susceptibility class and number of observed landslides has been convincingly consistent with each other. The 'very high' susceptibility class comprising only 2.99% of the total area accounted for 20.52% of the observed landslides; for other susceptibility classes (high:30.4%, moderate:52.94%, and low:13.67%), the ratio has been 38.42, 36.44, 4.6 respectively (Fig. 11).

4.6. Landslide risk to population

Landslide risk can be better understood by overlaying population and built environment layers on landslide susceptibility map (UNISDR,

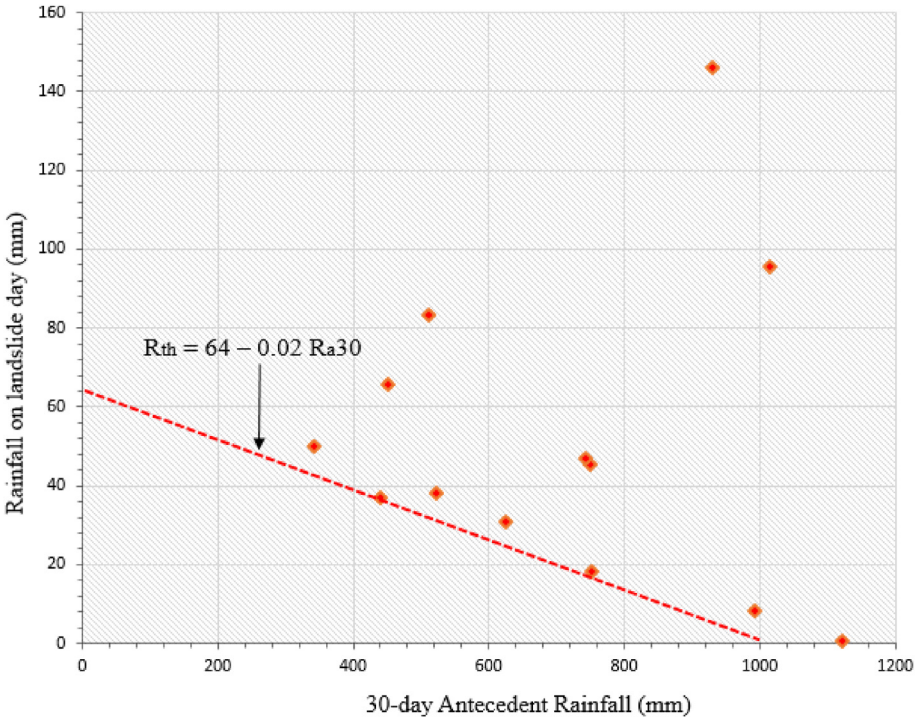

Fig. 8. Antecedent rainfall threshold for the Cox's Bazar district; R_{th} is the rainfall threshold and R_a30 is the 30-day antecedent rainfall.

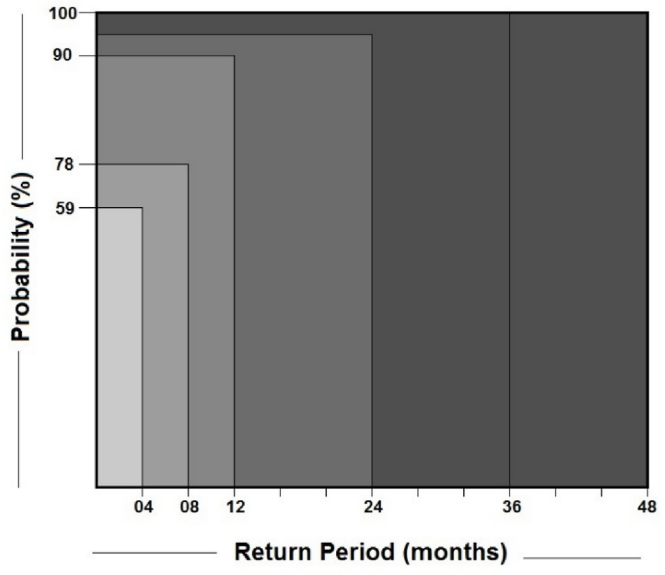

Fig. 9. Return period and probability of the future landslides in the Cox's Bazar District.

2017). The overlay analysis of the population data i.e., estimated total number of people per grid-cell (approximately 100m) and FR based landslide susceptibility scenario helped to map the landslide risk in the CBD. The landslide risk was identified as low (16.67%), moderate (53.89%), high (26.97%) and very high (2.45%) for the different parts of CBD, see Fig. 12. The results are based on the assumption that the areas with relatively high landslide susceptibility levels and high population density are at higher risk and vice versa. The use of gridded population data substantially reduces the distortion of in-situ information and generalization effects that usually occur due to administrative boundary based population data. The restriction of the risk analysis to populated areas also makes the prioritization for mitigation strategies easy and applicable. Few *Upazilas* of the CBD particularly Cox's Bazar-S, Chakaria, Pekua with high population size and density have the high concentration of the 'landslide risk' pixels. Pertinently, Kutubdia and western part of Maheshkhali have not been considered in this analysis. In addition, the Rohingya Refugee population, who are living a miserable life in temporary bamboo and tarpaulin shelters spread over the multiple clusters in the Ukhia and Teknaf *Upazilas* of the CBD has not been considered in the risk assessment process. The risk levels derived here are predominantly governed by the population density and areas even with gentle slope have some degree of landslide risk. Hence, while initiating the mitigation measures for reducing the landslide risk in the CBD based on the results of this study, the priority is to be given to the areas with 'very high' and 'high' risk levels.

4.7. *Rainfall threshold based landslide early warning system (LEWS)*

Based on derived landslide-triggering rainfall thresholds and the simulated susceptibility scenarios, this study proposes a cost-effective and convenient LEWS for the CBD (Fig. 13). The system uses information on amount of rainfall, time duration, and degree of susceptibility for projecting the likelihood of landslide occurrence. The probability of landslide occurrence remains 'negligible' in a scenario of 'very insignificant' (0–20%) rainfall within a 'very low' susceptible area and 'very high' if rainfall reaches the threshold (>90%) in a 'very high' susceptible area; the intermediate levels of the LEWS are described in Fig. 13. The information of rainfall thresholds and susceptibility can be combined and used to issue different levels of warning. The LEWS proposed here has a potential to help in minimizing the landslide impacts in the CBD and elsewhere.

5. Discussion

Owing to inherently complex nature of the landslides, forecasting their occurrence has never been an easy task. Two modeling approaches are generally adopted for the forecasting of landslides i.e., physically based and empirically based. Both the methods function at multiple

Table 4
Frequency ratio statistics.

Factor	Class	Frequency of pixels (%)	Frequency of landslides pixels (%)	FR
LULC	Built-up	10.02	14.70	1.46
	Waterbody	02.95	00.00	0.00
	Vegetation	56.47	43.65	0.77
	Bare land	03.79	16.94	4.46
	Cropland	26.75	24.79	0.92
Lithology				
	ava	07.76	07.10	0.91
	csd	19.09	05.83	0.30
	H2o	05.19	02.41	0.46
	Ppc	01.99	00.00	0.00
	QTdd	20.45	01.01	0.04
	QTdi	02.30	06.34	2.75
	QTdt	09.08	11.29	1.24
	QTg	08.48	05.71	0.67
	Tb	00.72	00.00	0.00
	Tbb	09.57	25.88	2.70
	Tt	15.32	34.39	2.24
Soil				
	Clay	26.97	11.96	0.44
	Loam	53.09	60.27	1.13
	Sand	02.18	02.93	1.34
	Sandy loam	13.42	08.91	0.66
	Silty loam	04.35	07.44	1.71
	Silty clay	04.29	07.22	1.68
	Silty clay loam	00.84	01.24	1.46
Slope				
	00–03.0	46.95	10.99	0.23
	03.5–06.5	32.55	36.92	1.13
	06.5–11.5	14.60	28.73	1.96
	11.5–20.5	05.08	10.43	2.05
	20.5–66.5	00.79	12.90	16.1
Aspect				
	Flat	07.24	12.00	1.65
	North	12.20	10.32	0.84
	Northeast	12.50	11.56	0.92
	East	10.30	11.44	1.11
	Southeast	12.77	09.76	0.76
	South	13.16	11.78	0.89
	Southwest	12.33	10.33	0.84
	West	09.65	11.44	1.18
	Northwest	09.80	11.22	1.14
Distance to streams (m)				
	0–500	57.41	37.59	0.65
	500–1000	29.00	20.08	0.69
	1000–1500	06.45	20.31	3.13
	1500–2000	07.11	21.99	3.09
Distance to faults (km)				
	0–8	25.39	23.45	0.92
	8–16	29.33	19.97	0.68
	16–24	28.04	19.86	0.70
	24–32	13.52	17.84	1.31
	32–40	03.69	18.85	5.09
Topographic Position Index (TPI)				
	TPI-1	01.83	13.46	7.35
	TPI-2	20.51	17.17	0.83
	TPI-3	64.25	34.68	0.53
	TPI-4	12.48	29.06	2.32
	TPI-5	00.91	05.61	6.14
Rainfall (mm)				
	1581–2268		08.97	0.61
	2668–2535		16.61	0.74
	2535–2868		19.97	0.89
	2868–3158		28.05	1.06
	3158–3680		26.37	1.80

spatial scales and use global, regional and local scales as units of analysis (Guzzetti et al., 2007). In the physically based approach, the triggering mechanism is simulated using maximum possible inputs, taking into consideration all the factors and each physical process that plays a role in landslide occurrence (Ascanio et al., 2012). The comprehensiveness of the physically based models though necessitates diverse spatial data inputs that control initiation of the landslides (Brunetti et al., 2010). Since the physically based models take into account dominant mechanical processes of landslides such as cohesion and friction angle, they have advantage of predicting the timing and location of the landslides (Wu et al., 2015). However, data required for the physically based models is generally unable or difficult to attain which often discourages their use. On the other hand, empirical models e.g., rainfall threshold calculations use statistical procedures for analysis that demand relatively less input data. For that reason, empirical models have been preferred tools for the prediction of rainfall induced slope failures and development of landslide early warning systems in different regions (Segoni et al., 2015; Robbins, 2016; Melillo et al., 2018). The analysis of this kind aims at understanding the relationship between the amount of the rainfall and landslides occurrence independent of landslide typology and scale.

Landslide inventories with spatiotemporal attributes and associated precipitation records form the foundation to derive landslide inducing rainfall thresholds for a particular region and for developing landslide early warning systems (Fell et al., 2008; Kirschbaum et al., 2009; Robbins, 2016; Fayne et al., 2019). The works of Campbell (1975) and Caine (1980) have been pioneering to establish such relationships between rainfall thresholds and landslide occurrence. A minimum threshold connotes the lowest amount of rainfall below which a landslide does not take place and the maximum threshold represents the amount above which a landslide always occurs (Guzzetti et al., 2007). However, not all of the rainfall values between the two thresholds trigger landslides; it is only when values approach the maximum threshold the probability of landslide occurrence increases (Glade et al., 2000). Comparison of the rainfall events that initiated landslides with the rainfall episodes without landslides are used to capture the thresholds (Valenzuela et al., 2019). In general, the thresholds are obtained by plotting rainfall amounts that resulted in landslides and identifying the lowest rainfall amount in the sequence.

The process of rainfall threshold determination makes use of information on observed landslides and respective rainfall in the area-of-interest to establish a relationship. The thresholds may not provide reliable estimates if the database on landslides is inadequate; longer time period covering maximum number of landslides including exact information related to their location and timing are essential for deriving empirically based rainfall thresholds. In other words, if the historical record of the landslides is not complete or not documented in the form of a reliable report for the selected time period, the derived thresholds can be misleading. One of the major drawbacks of the rainfall thresholds is that they are unable tell us about the exact location where a landslide is likely to occur. The vagueness in the location information of the expected landslides results in limited practical application of rainfall thresholds. Moreover, altered geomorphic conditions or human intervention such as slope destabilization from excavation, hill cutting for residential housing development, road construction or any other development projects may cause establishing minimum threshold not applicable for entire area even with homogenous topographic and lithological characteristics. In addition, most of the remote areas are ungauged and lack record of measured rainfall; under such circumstances rainfall data is extrapolated form the nearby areas or satellite based estimates are used. This situation can influence the accuracy of the rainfall thresholds. Despite issues associated with the process, the rainfall thresholds offer cost effective option for developing an operational LEWS.

Since rainfall based empirical threshold estimations consider the landslide occurrence entirely a function of precipitation, the spatial variability of factors like geology, slope, soil, vegetation, and stages of weathering are not considered. In order to add the dimension of landslide conditioning factors we carried out the landslide susceptibility analysis which can be used in combination with rainfall threshold estimates for reducing landslide impacts in the study area. The susceptibility analysis provides both quantitative and qualitative description of the possibility of occurrence and location of the landslides on the basis of various environmental conditions (Guzzetti et al., 2005). The process of landslide

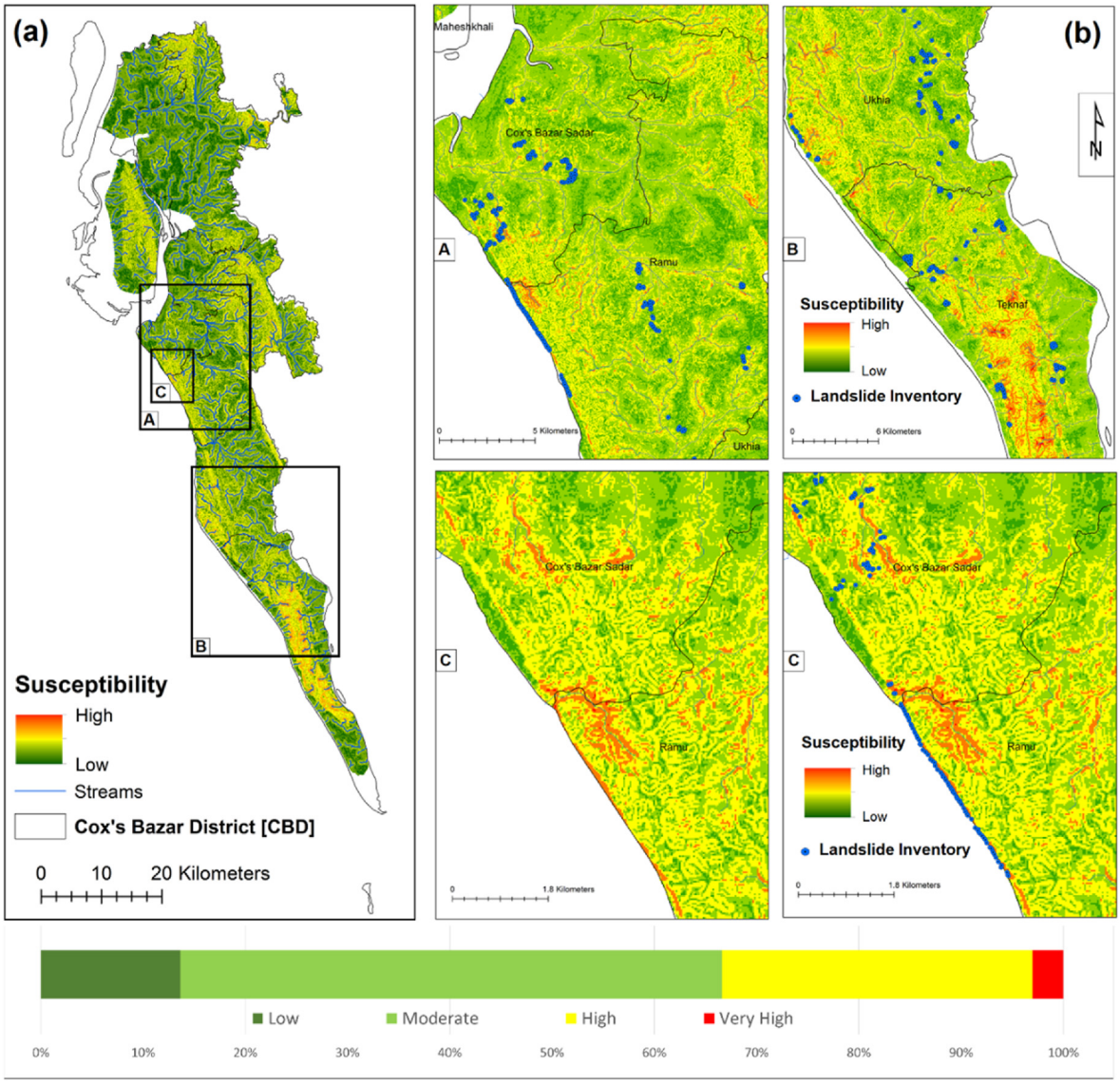

Fig. 10. Frequency Ratio (FR) based landslide susceptibility of the Cox's Bazar District.

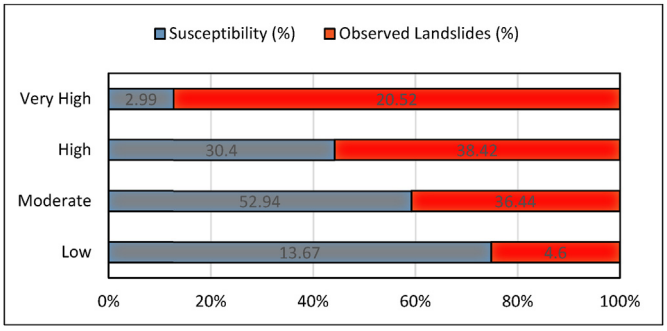

Fig. 11. Relative landslide density index depicting the ratio of susceptibility classes and number of landslides.

susceptibility analysis is dependent on complex data of slope movements and selection of the controlling factors, scale and adopted methodology (Ayalew and Yamagishi, 2005). Landslides susceptibility is usually simulated in space and time using empirical or physical models; and an area of interest is divided into different zones ranked according to varied probabilities of landslide occurrence (Guzzetti et al., 1999). The probabilities are established either on the basis of spatial components or derivation of return periods through the historical data based frequency analysis or comprehensively by combining the both (Glade, 2001). The factors that contribute to the landslide hazard are generally grouped into two types i.e., intrinsic and extrinsic elements; the intrinsic elements primarily include the inherent terrain properties such as geology and slope whereas extrinsic elements largely comprise rainfall and human interventions (Huabin et al., 2005). Probabilistic methods that use landslide inventory as an input may be considered as more reliable in quantitative risk assessment (Van Westen et al., 2006).

Landslide risk assessment (LRA) is an important dimension of landslide studies (Kanungo et al., 2008). Risk assessment is usually performed to identify the spots that are likely to experience relatively enhanced impacts from the future extreme events. The pre-event risk assessment offers an opportunity to understand the probability of loss in a given area and initiate the preparation measures and reduce the anticipated losses (Alam et al., 2019). Landslide risk assessment is essential for prevention and mitigation of landslide disasters (Anbalagan and Singh, 1996; Dai et al., 2002; Liu and Miao, 2018). In this investigation, instead of projecting the risk for the whole area which is not entirely inhibited we focused on the populated areas only to improve the applicability of the

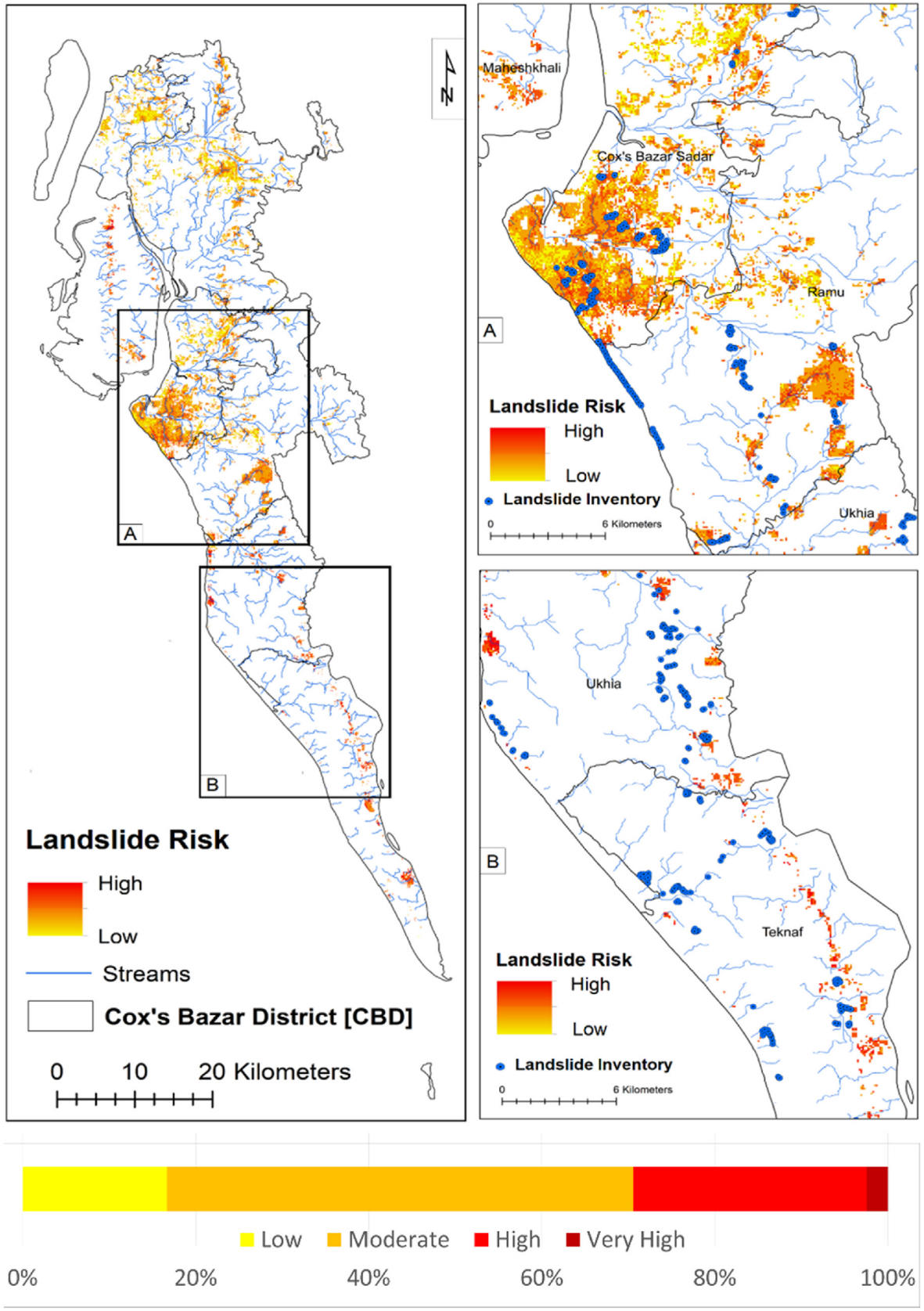

Fig. 12. Simulated landslide risk scenario of human settlement areas in the CBD.

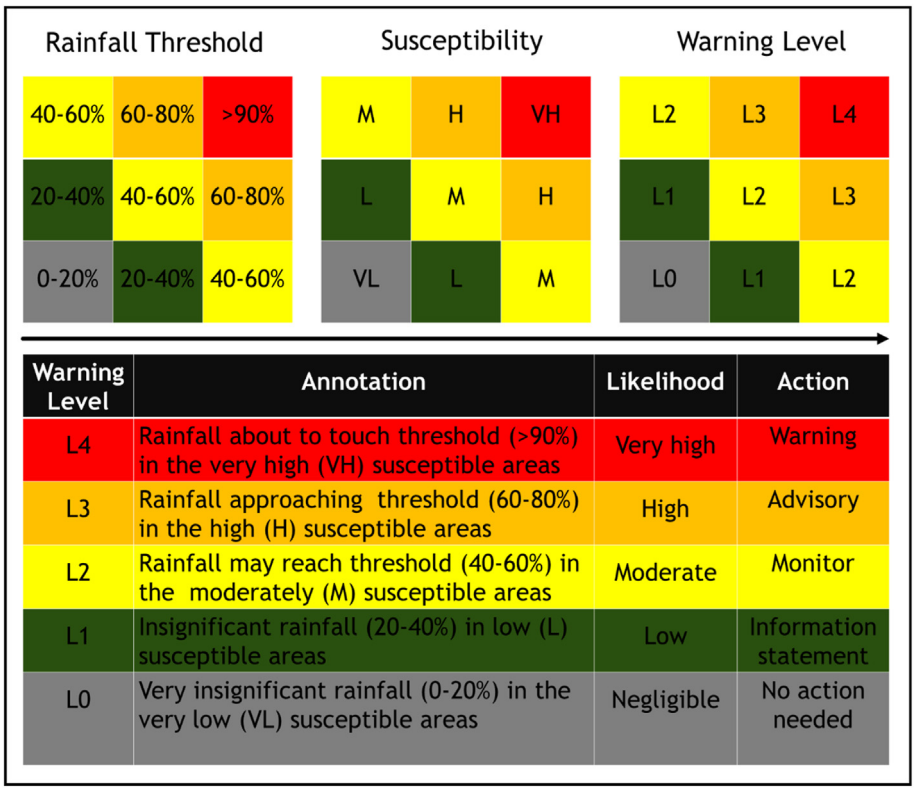

Warning Level	Annotation	Likelihood	Action
L4	Rainfall about to touch threshold (>90%) in the very high (VH) susceptible areas	Very high	Warning
L3	Rainfall approaching threshold (60-80%) in the high (H) susceptible areas	High	Advisory
L2	Rainfall may reach threshold (40-60%) in the moderately (M) susceptible areas	Moderate	Monitor
L1	Insignificant rainfall (20-40%) in low (L) susceptible areas	Low	Information statement
L0	Very insignificant rainfall (0-20%) in the very low (VL) susceptible areas	Negligible	No action needed

Fig. 13. Rainfall threshold based Landslide Early Warning System (LEWS) that can be adopted for the CDB.

results in context of landslide hazard mitigation. Geographic Information System (GIS) in combination with varied statistical techniques provides an effective environment for the assessment of risks related to various natural hazards including landslides. With a robust spatial data management structure, GIS exhibits exceptional capabilities to evaluate and integrate different elements of the risk (Alam et al., 2019, 2020; Taloor et al., 2023). For that reason, GIS has long been an integral part of hazard and risk assessment studies (Van Westen et al., 2006; Bhat et al., 2018, 2019).

6. Conclusions

The mountainous regions of South Asian countries characterize a global hotspot of landslide activity. One of such regions is the Cox's Bazar District (CBD), where frequently occurring landslides cause colossal loss of life and property almost every year. Incessant rainfall particularly during the monsoon season is the most common triggering factor of landslides in the district. Thus, evaluating the relationship between the observed landslides and rainfall patterns is useful for predicting the occurrence of future landslides and minimizing the associated impacts in the area. Considering the available information on fourteen landslide events and corresponding rainfall experienced during the period from 2003 to 2019, this study derived three different landslide-activating rainfall thresholds for the CBD. The recurrence interval of the landslides and their probabilities of occurrence were also assessed using antecedent rainfall threshold in the Poisson probability distribution, assuming landslide occurrence exclusively a function of rainfall. The study also encompassed landslide susceptibility analysis of the CBD considering ten spatially distributed conditioning factors. Frequency Ratio (FR) model was used for deriving the relative weight of the selected factors. The consistency check using relative landslide density index revealed that the FR model performed satisfactorily in projecting landslide susceptibility. The susceptibility map was subsequently integrated with population data to project the landslide risk scenario. The results of this analysis can be used in combination for issuing the warnings and reducing landslide impacts in the CBD. Moreover, the approach can be extended to other similar settings for mitigating the landslide hazard.

Declaration of competing interest

No competing interest is associated with this submission.

Acknowledgements

This research is funded by the Royal Society as part of the project, “Resilient Futures for the Rohingya Refugees” (Award Reference: CHL\R1\180288), supported under the UK Government's Global Challenges Research Fund. We thank Editor-in-Chief of Natural Hazards Research and the reviewers for their insightful comments which improved the quality and structure of this paper.

References

Ahmed, B., 2015. Landslide susceptibility modelling applying user-defined weighting and data driven statistical techniques in Cox's Bazar Municipality, Bangladesh. Nat. Hazards 79, 1707–1737.

Ahmed, B., 2017. Community Vulnerability to Landslides in Bangladesh [PhD Thesis]. University College London (UCL), London (UK).

Ahmed, B., Dewan, A., 2017. Application of bivariate and multivariate statistical techniques in landslide susceptibility modeling in Chittagong city corporation, Bangladesh. Rem. Sens. 9, 304. https://doi:10.3390/rs9040304.

Ahmed, B., Rahman, M.S., Sammonds, P., Islam, R., Uddin, K., 2020. Application of geospatial technologies in developing a dynamic landslide early warning system in a humanitarian context: the Rohingya refugee crisis in Cox's Bazar, Bangladesh. Geomatics, Nat. Hazards Risk 11 (1), 446–468. https://doi.org/10.1080/19475705.2020.1730988.

Ahsan, S., Bhat, M.S., Alam, A., Farooq, H., Shiekh, H.A., 2021. Evaluating the impact of climate change on extreme temperature and precipitation events over the Kashmir Himalaya. Clim. Dynam. https://doi.org/10.1007/s00382-021-05984-6.

Ahsan, S., Bhat, M.S., Alam, A., Sheikh, H.A., Farooq, H., 2023. Hydrological extremes and climatic controls on streamflow in Jhelum basin, NW Himalaya. Theor. Appl. Climatol. https://doi.org/10.1007/s00704-022-04346-4.

Alam, A., Sammonds, P., Ahmed, B., 2019. Cyclone risk assessment of the Cox's bazar and Rohingya refugee camps in southeast Bangladesh. Sci. Total Environ. 704, 135360. https://doi.org/10.1016/j.scitotenv.2019.135360.
Alam, A., Ahmed, B., Sammonds, P., 2020. Flash flood susceptibility assessment using the parameters of drainage basin morphometry in SE Bangladesh. Quat. Int. https://doi.org/10.1016/j.quaint.2020.04.047.
Alexander, D., 1992. On the causes of landslides: human activities, perception, and natural processes. Environ. Geol. Water Sci. 20, 165–179. https://doi.org/10.1007/BF01706160.
Ali, N., Alam, A., Bhat, M.S., Shah, B., 2022. Using historical data for developing a hazard and disaster profile of the Kashmir valley for the period 1900–2020. Nat. Hazards 114, 1609–1646. https://doi.org/10.1007/s11069-022-05440-6.
Anbalagan, R., Singh, B., 1996. Landslide hazard and risk assessment mapping of mountainous terrains — a case study from Kumaun Himalaya, India. Eng. Geol. 43 (4), 237–246. https://doi.org/10.1016/S0013-7952(96)00033-6.
Ascanio, R., Samuele, S., Filippo, C., Nicola, C., 2012. Statistical and environmental analyses for the definition of a regional rainfall threshold system for landslide triggering in Tuscany (Italy). J. Geogr. Sci. 22 (4), 617–629. https://doi.org/10.1007/s11442-012-0951-0.
Ayalew, L., Yamagishi, H., 2005. The application of GIS-based logistic regression for landslide susceptibility mapping in the Kakuda-Yahiko Mountains, Central Japan. Geomorphology 65, 15–31. https://doi.org/10.1016/j.geomorph.2004.06.010.
Baeza, C., Corominas, J., 2001. Assessment of shallow landslide susceptibility by means of multivariate statistical techniques. Earth Surf. Process. Landforms 26, 1251–1263. https://doi.org/10.1002/esp.263.
Baum, R.L., Fischer, S.J., Vigil, J.C., 2018. THRESH—software for tracking rainfall thresholds for landslide and debris-flow occurrence, user manual: U.S. Geological Survey Techniques and Methods 33. https://doi.org/10.3133/tm14A2 book 14, chap. A2.
Bhat, M.S., Alam, A., Ahmad, B., Kotlia, B.S., Farooq, H., Taloor, A.K., Ahmad, S., 2018. Flood frequency analysis of river jhelum in kashmir. Quat. Int. 507, 288–294. https://doi.org/10.1016/j.quaint.2018.09.039.
Bhat, M.S., Ahmad, B., Alam, A., Farooq, H., Ahmad, S., 2019. Flood hazard assessment of the Kashmir Valley using historical hydrology. Journal of Flood Risk Management 12 (Suppl. 1), e12521. https://doi.org/10.1111/jfr3.12521.
Bogaard, T., Roberto, G.R., 2018. Invited perspectives: hydrological perspectives on precipitation intensity-duration thresholds for landslide initiation: proposing hydro-meteorological thresholds. Nat. Hazards Earth Syst. Sci. 18, 31–39.
Brenning, A., 2008. Statistical geocomputing combining R and SAGA: the example of landslide susceptibility analysis with generalized additive models. In: Böhner, J., Blaschke, T., Montanarella, L. (Eds.), SAGA – Seconds Out (Hamburger Beiträge zur Physischen Geographie und Landschaftsökologie, 19, pp. 23–32.
Brunetti, M.T., Peruccacci, S., Rossi1, M., Luciani, S., Valigi, D., Guzzetti, F., 2010. Rainfall thresholds for the possible occurrence of landslides in Italy. Nat. Hazards Earth Syst. Sci. 10, 447–458.
Bui, D.T., Pradhan, B., Lofman, O., Revhaug, I., Dick, Ø.B., 2013. Regional prediction of landslide hazard using probability analysis of intense rainfall in the Hoa Binh province, Vietnam. Nat. Hazards 66, 707–730. https://doi.org/10.1007/s11069-012-0510-0.
Caine, N., 1980. The rainfall intensity–duration control of shallow landslides and debris flows. Geogr. Ann. A. 62, 23–27.
Campbell, R.H., 1975. Soil Slopes, Debris Flows, and Rainstorms in the Santa Monica Mountains and Vicinity, Southern California: U.S, 851. Geological Survey Professional Paper, p. 51.
Chauhan, S., Sharma, M., Arora, M.K., 2010. Landslide susceptibility zonation of the Chamoli region, Garhwal Himalayas, using logistic regression model. Landslides 7, 411–423. https://doi.org/10.1007/s10346-010-0202-3.
Chleborad, A.F., 2003. Preliminary Evaluation of a Precipitation Threshold for Anticipating the Occurrence of Landslides in the Seattle, Washington Area. USGS Open-File Report 03-463. U.S. Geological Survey, Reston, p. 17.
Crovelli, R.A., 2000. Probability models for estimation of number and costs of landslides. United States geological survey open file report 00-249. http://pubs.usgs.gov/of/2000/ofr-00-0249/ProbModels.html.
Dai, F.C., Lee, C.F., Ngai, Y.Y., 2002. Landslide risk assessment and management: an overview. Eng. Geol. 64 (1), 65–87. https://doi.org/10.1016/S0013-7952(01)00093-X.
Das, I., Stein, A., Kerle, N., Dadhwal, V.K., 2011. Probabilistic landslide hazard assessment using homogeneous susceptible units (HSU) along a national highway corridor in the northern Himalayas, India. Landslides 8, 293–308. https://doi.org/10.1007/s10346-011-0257-9.
Dikshit, A., Satyam, N., Pradhan, B., Kushal, S., 2020. Estimating rainfall threshold and temporal probability for landslide occurrences in Darjeeling Himalayas. Geosci. J. https://doi.org/10.1007/s12303-020-0001-3.
Dunbar, B., 2019. Brian Dunbar. https://www.nasa.gov/feature/nasa-data-helps-assess-landslide-risk-in-rohingya-refugee-camps. (Accessed 10 November 2020).
Fayne, J.V., Ahamed, A., Roberts-Pierel, J., Rumsey, A.C., Kirschbaum, D., 2019. Automated satellite-based landslide identification product for Nepal. Earth Interact. 23. https://doi.org/10.1175/EI-D-17-0022.1.
Fell, R., Corominas, J., Bonnard, C., Cascini, L., Leroi, E., Savage, W.Z., 2008. Guidelines for landslide susceptibility, hazard and risk zoning for land-use planning. Eng. Geol. 102, 99–111. https://doi.org/10.1016/j.enggeo.2008.03.014.
Gariano, S.L., Guzzetti, F., 2016. Landslides in a changing climate. Earth Sci. Rev. 162, 227–252.
Glade, T., 2001. Landslide hazard assessment and historical landslide data — an inseparable couple? In: Glade, T., Albini, P., Francés, F. (Eds.), The Use of Historical Data in Natural Hazard Assessments, Advances in Natural and Technological Hazards Research, 17. Springer, Dordrecht. https://doi.org/10.1007/978-94-017-3490-5_12.
Glade, T., Crozier, M., Smith, P., 2000. Applying probability determination to refine landslide-triggering rainfall thresholds using an empirical "Antecedent daily rainfall model. Pure Appl. Geophys. 157, 1059–1079.
GSB, 1990. In: Khurshid Alam, Md, Hasan, A.K.M.Shahidul, Khan, Mujibur Rahman (Eds.), Geological Map of Bangladesh (Geological Survey of Bangladesh), and John W. Whitney (United States Geological Survey), scale 1:1,000,000, published by Geological Survey of Bangladesh in 1990.
Guha-Sapir, D., Below, R., Hoyois, P.H., 2018. EM-DAT: International Disaster Database. Université Catholique de Louvain, Brussels, Belgium available at: http://www.emdat.be.
Guzzetti, F., Carrara, A., Cardinali, M., Reichenbach, P., 1999. Landslide hazard evaluation: a review of current techniques and their application in a multi-scale study, Central Italy. Geomorphology 31, 181–216.
Guzzetti, F., Reichenbach, P., Cardinali, M., Galli, M., Ardizzone, F., 2005. Probabilistic landslide hazard assessment at the basin scale. Geomorphology 72, 272–299. https://doi.org/10.1016/j.geomorph.2005.06.002.
Guzzetti, F., Peruccacci, S., Rossi, M., Stark, C.P., 2007. Rainfall thresholds for the initiation of landslides in central and southern Europe. Meteorog Atmos Phys 98, 239–267. https://doi.org/10.1007/s00703-007-0262-7.
Haque, U., Silva, P.F. da, Devoli, G., Pilz, J., Zhao, B., Khaloua, A., Wilopo, W., Andersen, P., Lu, P., Lee, J., Yamamoto, T., Keellings, D., Wu, J.H., Glass, G.E., 2019. The human cost of global warming: deadly landslides and their triggers (1995–2014). Sci. Total Environ. 682, 673–684. https://doi.org/10.1016/j.scitotenv.2019.03.415.
Huabin, W., Gangjun, L., Weiya, X., Gonghui, W., 2005. GIS-based landslide hazard assessment: an overview. Prog. Phys. Geogr. 29 (4), 548–567. https://doi.org/10.1191/0309133305pp462ra.
Huang, F., Yao, C., Liu, W., Li, Y., Liu, X., 2018. Landslide susceptibility assessment in the Nantian area of China: a comparison of frequency ratio model and support vector machine. Geomatics, Nat. Hazards Risk 9 (1), 919–938. https://doi.org/10.1080/19475705.2018.1482963.
Javier, Kumar, 2019. Frequency ratio landslide susceptibility estimation in a tropical mountain region. Int. Arch. Photogram. Rem. Sens. Spatial Inf. Sci. XLII-3/W8, 2019. Gi4DM 2019 – GeoInformation for Disaster Management, 3–6 September 2019, Prague, Czech Republic.
Kanungo, D.P., Arora, M.K., Gupta, R.P., 2008. Landslide risk assessment using concepts of danger pixels and fuzzy set theory in Darjeeling Himalayas. Landslides 5, 407–416. https://doi.org/10.1007/s10346-008-0134.
Khan, Y.A., Lateh, H., Baten, M.A., Kamil, A.A., 2012. Critical antecedent rainfall conditions for shallow landslides in Chittagong City of Bangladesh. Environ. Earth Sci. 67, 97–106. https://doi.org/10.1007/s12665-011-1483-0.
Kirschbaum, D.B., Adler, R., Hong, Y., Lerner-Lam, A., 2009. Evaluation of a preliminary satellite-based landslide hazard algorithm using global landslide inventories. Nat. Hazards Earth Syst. Sci. 9, 673–686. https://doi.org/10.5194/nhess-9-673-2009.
Lee, S., 2005. Application of logistic regression model and its validation for landslide susceptibility mapping using GIS and remote sensing data. Int. J. Rem. Sens. 26 (7), 1477–1491. https://doi.org/10.1080/01431160412331331012.
Lee, S., Pradhan, B., 2007. Landslide hazard mapping at Selangor, Malaysia using frequency ratio and logistic regression models. Landslides 4, 33–41. https://doi.org/10.1007/s10346-006-0047-y.
Lee, S., Sambath, T., 2006. Landslide susceptibility mapping in the Damrei Romel area, Cambodia using frequency ratio and logistic regression models. Environ. Geol. 50, 847–855. https://doi.org/10.1007/s00254-006-0256-7.
Lin, L., Lin, Q., Wang, Y., 2017. Landslide susceptibility mapping on a global scale using the method of logistic regression. Nat. Hazards Earth Syst. Sci. 17, 1411–1424. https://doi.org/10.5194/nhess-17-1411-2017.
Liu, X., Miao, C., 2018. Large-scale assessment of landslide hazard, vulnerability and risk in China. Geomatics, Nat. Hazards Risk 9 (1), 1037–1052. https://doi.org/10.1080/19475705.2018.1502690.
Lombardo, L., Mai, P.M., 2018. Presenting logistic regression-based landslide susceptibility results. Eng. Geol. 244, 14–24. https://doi.org/10.1016/j.enggeo.2018.07.019.
Martinović, K., Gavin, K., Reale, C., Mangan, C., 2018. Rainfall thresholds as a landslide indicator for engineered slopes on the Irish Rail network. Geomorphology 306, 40–50. https://doi.org/10.1016/j.geomorph.2018.01.006.
Mathew, J., Babu, D.G., Kundu, S., Kumar, K.V., Pant, C.C., 2014. Integrating intensity–duration-based rainfall threshold and antecedent rainfall-based probability estimate towards generating early warning for rainfall-induced landslides in parts of the Garhwal Himalaya, India. Landslides 11, 575–588. https://doi.org/10.1007/s10346-013-0408-2.
Melillo, M., Brunetti, M.T., Peruccacci, S., Gariano, S.L., Roccati, A., Guzzetti, F., 2018. A tool for the automatic calculation of rainfall thresholds for landslide occurrence. Environ. Model. Software 105, 230–243. https://doi.org/10.1016/j.envsoft.2018.03.024.
NASA Earth Observatory, 2020. Climate Change Could Trigger More Landslides in High Mountain Asia. https://www.nasa.gov/feature/goddard/2020/climate-change-could-trigger-more-landslides-in-high-mountain-asia.
Park, S., Choi, C., Kim, B., et al., 2013. Landslide susceptibility mapping using frequency ratio, analytic hierarchy process, logistic regression, and artificial neural network methods at the Inje area, Korea. Environ. Earth Sci. 68, 1443–1464. https://doi.org/10.1007/s12665-012-1842-5.
Park, J.Y., Lee, S.R., Lee, D.H., Kim, Y.T., Lee, J.S., 2019. A regional-scale landslide early warning methodology applying statistical and physically based approaches in sequence. Eng. Geol. 260, 105193. https://doi.org/10.1016/j.enggeo.2019.105193.

Petley, D., 2012. Global patterns of loss of life from landslides. Geology 40 (10), 927–930. https://doi.org/10.1130/G33217.1.

Poudyal, C.P., Chang, C., Oh, H.J., et al., 2010. Landslide susceptibility maps comparing frequency ratio and artificial neural networks: a case study from the Nepal Himalaya. Environ. Earth Sci. 61, 1049–1064. https://doi.org/10.1007/s12665-009-0426-5, 2010.

Rahman, G., Rahman, A.U., Bacha, A.S., Mahmood, S., 2020. Assessment of landslide susceptibility using weight of evidence and frequency ratio model in shahpur valley, eastern hindu kush. Nat. Hazards Earth Syst. Sci. https://doi.org/10.5194/nhess-2020-167.

Robbins, J.C., 2016. A probabilistic approach for assessing landslide-triggering event rainfall in Papua New Guinea, using TRMM satellite precipitation estimates. J. Hydrol. 541296–541309. https://doi.org/10.1016/j.jhydrol.2016.06.052.

Sarwar, G.M., 2008. Landslide Tragedy of Bangladesh, the First World Landslide Forum, 18-21 November 2008. United Nations University (UNU), Tokyo, Japan.

Schuster, R.L., Highland, L.M., 2001. Socioeconomic and Environmental Impacts of Landslides in the Western Hemisphere. U.S. Geological Survey Open-File Report 01-0276. https://pubs.usgs.gov/of/2001/ofr-01-0276/.

Segoni, S., Battistini, A., Rossi, G., Rosi, A., Lagomarsino, D., Catani, F., Moretti, S., Casagli, N., 2015. Technical Note: an operational landslide early warning system at regional scale based on space–time-variable rainfall thresholds. Nat. Hazards Earth Syst. Sci. 15, 853–861.

Sengupta, A., Gupta, S., Anbarasu, K., 2010. Rainfall thresholds for the initiation of landslide at Lanta Khola in north Sikkim, India. Nat. Hazards 52, 31–42. https://doi.org/10.1007/s11069-009-9352-9.

Shah, B., Sultan Bhat, M., Alam, A., Ali, N., 2022. Developing landslide hazard scenario using the historical events for the Kashmir Himalaya. Nat. Hazards 114, 3763–3785. https://doi.org/10.1007/s11069-022-05542-1, 2022.

Shahabi, H., Hashim, M., 2015. Landslide susceptibility mapping using GIS-based statistical models and Remote sensing data in tropical environment. Sci. Rep. 5, 9899. https://doi.org/10.1038/srep09899.

Solaimani, K., Mousavi, S.Z., Kavian, A., 2013. Landslide susceptibility mapping based on frequency ratio and logistic regression models. Arabian J. Geosci. 6, 2557–2569. https://doi.org/10.1007/s12517-012-0526-5.

Sultana, N., 2020. Analysis of landslide-induced fatalities and injuries in Bangladesh: 2000-2018. Cogent Soc. Sci. 6 (1), 1737402. https://doi.org/10.1080/23311886.2020.1737402.

Taloor, A.K., Kothyari, G.C., Dumka, R.K., Alam, A., Malik, K., 2023. Crustal deformation study of Kashmir basin: insights from PSInSAR based time series analysis. J. Appl. Geophys. 211. https://doi.org/10.1016/j.jappgeo.2023.104979.

UNISDR, 2017. Landslide Hazard and Risk Assessment. Words into Action Guidelines: National Disaster Risk Assessment Hazard Specific Risk Assessment. https://www.unisdr.org/files/52828_03landslidehazardandriskassessment.pdf.

Valenzuela, P., Zêzere, J.L., Domínguez-Cuesta, M.J., García, M.A.M., 2019. Empirical rainfall thresholds for the triggering of landslides in Asturias (NW Spain). Landslides 16, 1285–1300. https://doi.org/10.1007/s10346-019-01170-2.

Van Westen, C.J., Van Asch, T.W.J., Soeters, R., 2006. Landslide hazard and risk zonation—why is it still so difficult? Bull. Eng. Geol. Environ. 65, 167–184. https://doi.org/10.1007/s10064-005-0023-0.

Van Westen, C.J., Jaiswal, P., Ghosh, S., Martha, T.R., Sekhar, L.K., 2012. Landslide inventory, hazard and risk assessment in India. In: Terrigenous Mass Movements. https://doi.org/10.1007/978-3-461642-25495-6_9.

Varnes, D.J., 1978. Slope movement types and processes. In: Schuster, R.L., Krizek, R.J. (Eds.), Landslides, Analysis and Control, Special Report 176: Transportation Research Board. National Academy of Sciences, Washington, DC, pp. 11–33.

Wang, L.-J., Sawada, K., Moriguchi, S., 2013. Landslide susceptibility analysis with logistic regression model based on FCM sampling strategy. Comput. Geosci. 57, 81–92. https://doi.org/10.1016/j.cageo.2013.04.006.

Wu, Y., Lan, H., Gao, X., Li, L., Yang, Z., 2015. A simplified physically based coupled rainfall threshold model for triggering landslides. Eng. Geol. 195, 63–69. https://doi.org/10.1016/j.enggeo.2015.05.022.

Yesilnacar, E., Topal, T., 2005. Landslide susceptibility mapping: a comparison of logistic regression and neural networks methods in a medium scale study, Hendek region (Turkey). Eng. Geol. 79 (3–4), 251–266. https://doi.org/10.1016/j.enggeo.2005.02.002.

Yilmaz, I., 2009. Landslide susceptibility mapping using frequency ratio, logistic regression, artificial neural networks and their comparison: a case study from Kat landslides (Tokat—Turkey). Comput. Geosci. 35, 1125–1138. https://doi.org/10.1016/j.cageo.2008.08.007.